Rare Metal Materials and Engineering
Volume 52, Issue 7, July 2023
Available online at www.rmme.ac.cn

Science Press

Cite this article as: Song Boyu, Han Yongquan, Cheng Juan, et al. Effect of Sn Doping on Magnetocaloric Effect and Phase Transition Properties of (La, Ce) (Fe, Al, Si)$_{13}$ Alloys[J]. Rare Metal Materials and Engineering, 2023, 52(07): 2335-2342.

ARTICLE

Effect of Sn Doping on Magnetocaloric Effect and Phase Transition Properties of (La, Ce)(Fe, Al, Si)$_{13}$ Alloys

Song Boyu[1,2,3], Han Yongquan[1,3], Cheng Juan[4], Gao Lei[4], Liu Cuilan[4], Huang Jiaohong[4]

[1] Inner Mongolia University of Technology, Hohhot 010051, China; [2] Baotou Vocational and Technical College, Baotou 014030, China; [3] Engineering Research Center of Development and Processing Protection of Advanced Light Metals, Ministry of Education, Hohhot 010051, China; [4] State Key Laboratory of Baiyunobo Rare Earth Resource Researches and Comprehensive Utilization, Baotou 014030, China

Abstract: The magnetocaloric effect and phase transition properties of $La_{0.75}Ce_{0.25}Fe_{11.5-x}Al_{0.2}Si_{1.3}Sn_x$ (x=0, 0.05, 0.1, 0.2, wt%) alloys were investigated. X-ray diffraction results show that with increasing the Sn doping content, the content of 1∶13 main phase is decreased, and the content of α-Fe and LaFeSi phases is increased. By combining the density functional theory with experimental results, it is found that increasing the Sn doping content can increase the lattice constant and enhance the exchange interactions between adjacent atoms, thereby increasing the Curie temperature. When the magnetic field is 2 T, the maximum magnetic entropy change in the system is 13.59 $J\cdot kg^{-1}\cdot K^{-1}$ and its relative cooling power is 154 J/kg, showing great potential as magnetic refrigeration material. Based on the Banerjee criterion and the field dependence index n of isothermal entropy change, it is concluded that when the Sn doping content is 0.05wt%, the first-order phase transition changes to the second-order phase transition of the alloy. The phase transition behavior of the alloy is very sensitive to the Sn content, and multi-stage series refrigeration can be achieved by adjusting the doping content.

Key words: magnetocaloric effect; LaFeSi; phase transition

Because gas-compression refrigeration suffers from the non-environmentally friendly refrigeration process and low refrigeration efficiency, magnetic refrigeration technology has been proposed based on the magnetocaloric effect (MCE), which has the advantages of energy saving, high efficiency, environment protection, stability, and reliability, showing great potential in the refrigeration industry[1–3]. In the MCE-based magnetic refrigeration technology, the magnetic moment of the magnetocaloric material remains ordered or disordered along the direction of magnetic field with or without an external magnetic field, so the entropy of the system changes, resulting in the heat absorption and discharge[4–5]. MCE is related to the first-order magnetic transition (FOMT) and the second-order magnetic transition (SOMT). According to Ehrenfest classification, FOMT feature is the discontinuity of the first derivative of free energy related to the thermodynamic parameters, and the discontinuity of the second derivative of free energy corresponds to SOMT feature[6]. Generally, magnetocaloric materials with FOMT characteristics have large MCE, relatively narrow temperature range, and thermal or magnetic hysteresis. Conversely, the magnetocaloric materials with SOMT characteristics exhibit small MCE and relatively wide temperature range without thermal or magnetic hysteresis.

Magnetocaloric materials include Gd[7], La(Fe, Si)$_{13}$[8], GdSiGe[9], MnAs[10], Heuslers alloys[11], and FeRh[12]. As a typical second-order magnetic phase transition material, Gd is usually used in the magnetic refrigerators. However, the magnetocaloric properties of Gd are sensitive to the purity. High-purity Gd is expensive, and its Curie temperature is not adjustable, which seriously restricts its application. Among the first-order magnetic phase transition materials, the La(Fe, Si)$_{13}$ alloy is non-toxic and exhibits large magnetic entropy change and adjustable Curie temperature. In addition, the preparation

Received date: March 01, 2023
Foundation item: National Natural Science Foundation of China (52066001); Science and Technology Plan Project of Inner Mongolia Autonomous Region (2020GG0313); Inner Mongolia Natural Science Foundation Project (2021MS05016); Research Program of Science and Technology at Universities of Inner Mongolia Autonomous Region of China (NJZY22119); Northern Rare Earth Project (BFXT-2021-D-0013)
Corresponding author: Han Yongquan, Ph. D., Professor, School of Materials Science and Engineering, Inner Mongolia University of Technology, Hohhot 010051, P. R. China, Tel: 0086-471-6575752, E-mail: hyq@imut.edu.cn

cost of La(Fe, Si)$_{13}$ alloy is relatively small, presenting great application potential[13]. MCE and phase transition properties of La(Fe, Si)$_{13}$ alloy can be greatly changed by adjusting the element proportion or doping elements. For the La(Fe, Si)$_{13}$ alloy, when Si content≤1.6wt%, the alloy exhibits the first-order phase transition (FOPT) characteristics; when Si content ≥2wt%, the alloy exhibits the second-order phase transition (SOPT) characteristics; the $NaZn_{13}$ cubic structure remains unchanged[14–15]. Lin et al doped Mn into the $La_{0.8}Ce_{0.2}Fe_{11.4-x}Mn_xSi_{1.6}$ alloy. With increasing the Mn content from 0wt% to 0.3wt%, the alloy shows FOPT, the transition temperature is decreased from 177 K to 121 K, and the relative cooling power (RCP) remains as a large constant under magnetic field of 1 T[16]. After partially replacing Fe with Co atoms, the phase transition changes from FOPT to SOPT when Co content=0.4wt%, and the Curie temperature (T_C) shifts to higher temperatures with maintaining the large MCE[17–18]. Nb[19] and Gd[20] have been doped into the La(Fe, Si)$_{13}$ alloy. With increasing their doping content, the magnetic entropy change is decreased, T_C is increased, and the hysteresis loss is eliminated. When Nb content is 4wt% and Gd content is 7wt%, the phase transition changes from FOPT to SOPT. Hu et al[21] prepared La(Fe_xAl_{1-x})$_{13}$ alloys and found that when x=0.86, the alloy is soft ferromagnetic, and the phase transition from paramag-netic state to the ferromagnetic state is SOPT. FOPT occurs at x=11.18 – 11.96. Additionally, the density functional theory (DFT) has been proposed and it is commonly used to analyze the effect of doping elements in La(Fe, Si)$_{13}$ alloys. Dai et al[22] used DFT to reconstruct the $LaFe_{11.6}Si_{1.4}$ alloy doped with B and C, and found that the magnetic-transition behavior is related to the Fe-Fe bond. Moreno-Ramírez et al[23–24] studied MCE and phase transition sequence of the La(Fe, Si)$_{13}$ alloy doped with Ni and Cr of different contents by DFT and experiments. DFT results are consistent with the experimental ones. Doping Ni and Cr cannot significantly change the crystal structure and total magnetic moment. Besides, when Ni>0.21wt% and Cr>0.53wt%, the phase transition changes from FOPT to SOPT. Therefore, it is very important to evaluate the effects of different doping elements on MCE and phase transition properties of alloys, providing application guidance for the magnetocaloric materials.

Doping or substituting elements with similar chemical properties is a common method to improve the comprehensive properties of materials[25]. Sn and Si belong to the same group of elements in the periodic table, thereby presenting similar chemical properties. The Sn doping in $Gd_5Si_2Ge_2$ magnetic refrigeration materials increases the Curie temperature and expands the refrigeration temperature range while maintaining the magnetocaloric effect[26]. However, the effect of Sn doping in La(Fe, Si)$_{13}$ alloy is rarely investigated. In this research, Sn was doped in the (La, Ce) (Fe, Al, Si)$_{13}$ alloy[27] with high magnetic entropy change and refrigeration capacity. DFT calculations were conducted to investigate the exchange interaction between the magnetic atoms, and the Curie temperature, isothermal magnetic entropy change, and phase transition properties of the alloy were investigated through experiments.

1 Experiment

The industrially pure raw materials (99.5wt% La, 99.5wt% Ce, 99wt% Fe, 99.7wt% Al, 99.9wt% Si, and 99.7wt% Sn) were used. $La_{0.75}Ce_{0.25}Fe_{11.5-x}Al_{0.2}Si_{1.3}Sn_x$ (x=0, 0.05, 0.1, 0.2, wt%) alloys were prepared by melting under the protection of argon gas in a high-frequency induction furnace. Each raw metal of 70 g was used for melting (excess 5wt% La and 5wt% Ce were added to compensate for the volatilization of La and Ce during melting). To ensure the uniform composition of alloy specimens, each specimen was turned and melted three times. Then, they were placed in a sintering furnace, heat-treated at 1090 ° C for 144 h under argon protection, and water quenched. X-ray diffractometer (XRD, X'Pert PRO diffractometer) was used to analyze the phases of crushed specimens, and XRD patterns were treated by Rietveld refinement through Maud software. The magnetic properties of the specimens of approximately 20 mg were measured by LakeShore7407 vibrating specimen magnetometer. The magnetic entropy (ΔS_M) values of the alloys were calculated by Maxwell equation, and the magnetocaloric properties were analyzed.

2 Results and Discussion

2.1 Structural characterization

XRD patterns of $La_{0.75}Ce_{0.25}Fe_{11.5-x}Al_{0.2}Si_{1.3}Sn_x$ (x=0, 0.05, 0.1, 0.2) alloys are shown in Fig.1.

The $La_{0.75}Ce_{0.25}Fe_{11.5-x}Al_{0.2}Si_{1.3}Sn_x$ alloy with x=0 is mainly composed of the 1:13 phase and a small amount of α-Fe phase (2θ=45°). With increasing the Sn doping content, the peak of α-Fe phase gradually becomes more obvious, and the corresponding peak of LaFeSi also appears. The analysis results based on XRD patterns are shown in Table 1. With increasing the Sn doping content, the content of 1: 13 main phase is gradually decreased, and the contents of α-Fe and LaFeSi phases are gradually increased. Additionally, because the Sn radius (0.141 nm) is larger than that of Fe atom (0.117 nm), the lattice constant is monotonically increased with increasing the Sn doping content, indicating that the Sn atoms replace the Fe atoms. The variation in lattice constant depends on the content of doping element in the alloy.

2.2 Lattice parameter and Curie temperature

CASTEP module of Materials Studio was used to calculate the electronic structures of $La_{0.75}Ce_{0.25}Fe_{11.5-x}Al_{0.2}Si_{1.3}Sn_x$ alloys

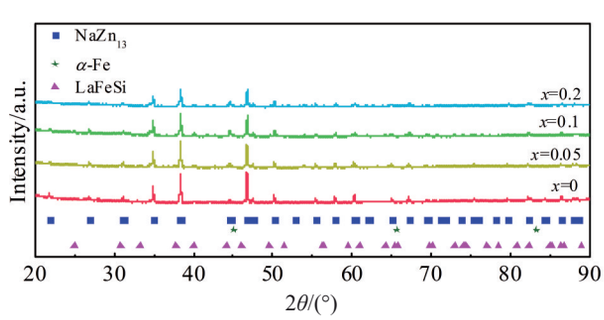

Fig.1 XRD patterns of $La_{0.75}Ce_{0.25}Fe_{11.5-x}Al_{0.2}Si_{1.3}Sn_x$ alloys

Table 1 Lattice constant, phase proportions, *R*-weighted pattern factor (R_{wp}), *R*-Bragg factor (R_b), *R*-expected factor (R_{exp}), and goodness of fit (GOF) of $La_{0.75}Ce_{0.25}Fe_{11.5-x}Al_{0.2}Si_{1.3}Sn_x$ alloys after Rietveld refinement

Parameter	x=0	x=0.05	x=0.1	x=0.2
Experimental lattice constant, a_{exp}/nm	1.1471	1.1475	1.1477	1.1483
DFT-simulated lattice constant, a_{DFT}/nm	1.1428	1.1550	1.1639	1.1798
Lattice constant error/%	0.37	0.65	1.41	2.74
1:13 phase content/wt%	96.4	90.7	89.7	89.5
α-Fe phase content/wt%	3.6	6.6	7.7	7.9
LaFeSi phase content/wt%	0.0	2.7	2.5	2.6
R-weighted pattern factor, R_{wp}/%	2.582	2.594	2.604	2.833
R-Bragg factor, R_b/%	1.926	1.955	1.956	2.103
R-expected factor, R_{exp}/%	1.899	1.995	1.995	1.993
GOF	1.359	1.300	1.305	1.421

based on DFT framework by Ceperley, Alder, Perdew, and Zunger exchange-correlation functions[28–31] with the local density approximation and plane wave cutoff energy of 335 eV[32] in 7×7×7 k-point mesh. The self-consistent field precision is less than 1×10^{-7} eV/atom, the atomic interaction force is less than 0.05 eV/nm, and all calculations include the collinear spin polarization. Cell construction was based on the ideal cell of $NaZn_{13}$-type La(Fe, Si)$_{13}$ (space group Fm3c), where the La atom occupies the Wyckoff position at 8a(1/4, 1/4, 1/4) sites, the Fe^{I} atom is located at 8b(0, 0, 0) sites, and the Fe^{II} or Si atom is located at 96i(0, *y*, *z*) sites. The lattice constant of intrinsic $LaFe_{11.5}Si_{1.5}$ alloy is 1.1411 nm, and the error is only 0.46%, compared with the experimental value[33]. Construction of Sn-doped structures was then performed. Based on the assumption that the doped Sn atom in La(Fe, Si)$_{13}$ alloy is at the 96i or 8b atomic position, the separate energy calculations were conducted. It is found that the Sn atom prefers to occupy the 96i position. According to Ref. [34], the preferred position of Al atom in the cell is 96i. Therefore, not only Fe^{II} and Si atoms, but also Al and Sn atoms exist at the 96i position. The proportion of different atoms at 96i position can be calculated by dividing the total mass ratio of an element by its relative atomic mass ratio. For example, the $LaFe_{11.5}Si_{1.5}$ alloy is composed of cells of 87.5wt% Fe^{II} and 12.5wt% Si. The lattice constants of $LaFe_{11.5-x}Al_{0.2}Si_{1.3}Sn_x$ (x=0, 0.05, 0.1, 0.2) simulated cells corresponding to the $La_{0.75}Ce_{0.25}Fe_{11.5-x}Al_{0.2}Si_{1.3}Sn_x$ (x=0, 0.05, 0.1, 0.2) alloys were then calculated. The lattice constants of the alloys with different Sn contents obtained by Rietveld refinement and DFT calculation are shown in Fig. 2. The change trends of lattice constant from DFT calculation and Rietveld refinement are in good agreement. With increasing the Sn content, the lattice constant calculated by DFT is increased, which leads to the narrowing of 3d band, the increase in interactions between the ferromagnetism, and the increase in Curie temperature[35].

It is widely known that the variation of Curie temperature not only influences the lattice constant, but also changes the magnetic interaction caused by expansion or contraction of the bonds between the atoms in crystal structure[36–37]. The

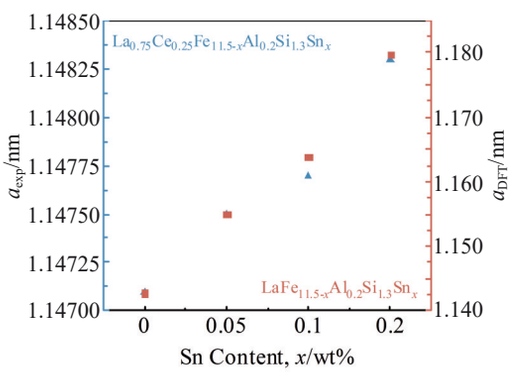

Fig.2 Lattice constants of $La_{0.75}Ce_{0.25}Fe_{11.5-x}Al_{0.2}Si_{1.3}Sn_x$ alloys obtained by Rietveld refinement and $LaFe_{11.5-x}Al_{0.2}Si_{1.3}Sn_x$ alloys obtained by DFT calculations

bond lengths of Fe-Fe atom pairs at five positions of the unit cell are shown in Fig. 3, where B1 is the Fe^{I}-Fe^{II}/Si/Al/(Sn) atom pair and B2–B5 are Fe^{II}/Si/Al/(Sn)-Fe^{II}/Si/Al/(Sn) atom pairs. The weighted average value of the Fe-Fe bond lengths represents the average Fe-Fe bond length[38]. If the elongation of the average Fe-Fe bond length is less than 0.255 nm or the shortening of average Fe-Fe bond length is greater than 0.255 nm, the exchange interaction will be strengthened and the exchange integral $J_{Fe\text{-}Fe}$ will be increased. Conversely, if the elongation of average Fe-Fe bond length is greater than 0.255 nm or the shortening of average Fe-Fe bond length is less than 0.255 nm, the exchange interaction will be weakened and the exchange integral $J_{Fe\text{-}Fe}$ will be decreased. The competition between the two opposite effects determines the variation of total $J_{Fe\text{-}Fe}$[39]. The measured results are shown in Fig. 4. With increasing the Sn doping content, the B1 and B5 bonds elongate by less than 0.255 nm, the B3 and B4 bonds elongate by greater than 0.255 nm, and the B2 bond contracts by greater than 0.255 nm. In addition, the variation of B1–B5 bonds is 0.0045, −0.0001, 0.006, 0.0157, and 0.0061 nm, respectively. Therefore, the average Fe-Fe bond length increases, which can enhance the exchange interaction between adjacent atoms. Besides, it is inferred that the total $J_{Fe\text{-}Fe}$ is increased with increasing the Sn doping content. With

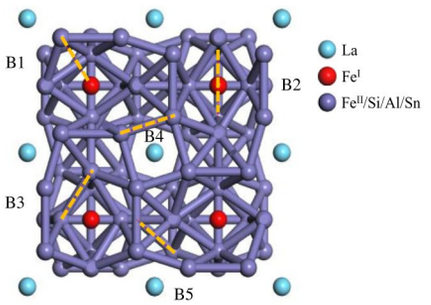

Fig.3 Fe-Fe bonds at different positions in $LaFe_{11.5-x}Al_{0.2}Si_{1.3}Sn_x$ (x=0, 0.05, 0.1, 0.2) alloys

larger total $J_{Fe\text{-}Fe}$, the bonds are easily parallel to each other after spin, which normally requires more thermal energy to disrupt the regular arrangement within the magnet, thereby increasing the Curie temperature.

2.3 Magnetocaloric properties and phase transition characteristics

The heating (cooling) curves of magnetic moment (M) - temperature (T) of $La_{0.75}Ce_{0.25}Fe_{11.5-x}Al_{0.2}Si_{1.3}Sn_x$ (x=0, 0.05, 0.1, 0.2) alloys under applied magnetic field of 0.05 T are shown in Fig.5.

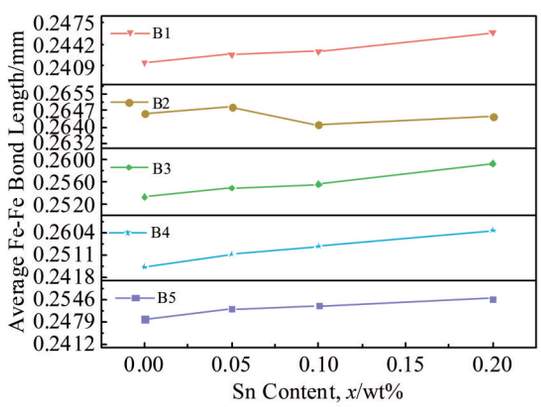

Fig.4 Relationship between Fe-Fe average bond length and Sn doping content of $LaFe_{11.5-x}Al_{0.2}Si_{1.3}Sn_x$ alloys

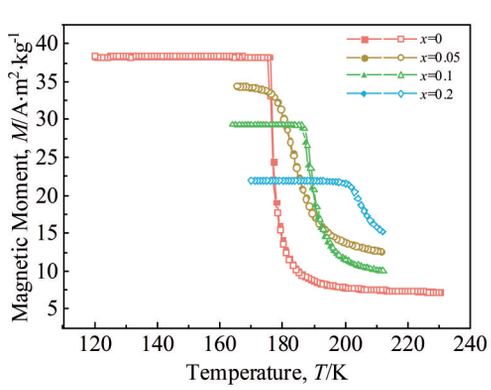

Fig.5 M-T curves of $La_{0.75}Ce_{0.25}Fe_{11.5-x}Al_{0.2}Si_{1.3}Sn_x$ alloys during heating (cooling) at magnetic field of 0.05 T

The M-T curve of the alloy with x=0 does not overlap with the front end of the M-T curve of cooling, and the thermal hysteresis occurs. Conversely, the M-T curves for the Sn-doped alloys overlap with those of cooling process, and almost no thermal hysteresis occurs. The Curie temperature is the critical temperature for the transition between the ferromagnetic and paramagnetic states, and it is defined as the minimum value from the relationship plot between the first derivative of magnetization and T. At x=0, 0.05, 0.1, and 0.2, the Curie temperature is 177, 184, 190, and 204 K, respectively, indicating that the Curie temperature is increased with increasing the Sn doping content. This result agrees well with the trend predicted by DFT calculations and the rule of periodic table: the elemental transition temperature is lower for the left-side elements of Fe (anti-ferromagnetic coupling) and higher for the right-side elements of Fe (ferromagnetic coupling)[40].

To measure the magnetocaloric properties of $La_{0.75}Ce_{0.25}Fe_{11.5-x}Al_{0.2}Si_{1.3}Sn_x$ (x=0, 0.05, 0.1, 0.2) alloys, the isothermal magnetic entropy change (ΔS_M) is calculated, as follows:

$$\Delta S_M = \int_0^H \left(\frac{\partial M}{\partial T}\right)_H dH \quad (1)$$

where H is the applied magnetic field, M is the magnetization, and T is the temperature.

The isothermal magnetic entropy change curves of $La_{0.75}Ce_{0.25}Fe_{11.5-x}Al_{0.2}Si_{1.3}Sn_x$ (x=0, 0.05, 0.1, 0.2) alloys under magnetic field of 2 T are shown in Fig.6. When the Sn doping content changes from 0wt% to 0.05wt%, ΔS_M is decreased from 13.59 J/(kg·K) to 6.08 J/(kg·K), the corresponding Curie temperature shifts towards the high-temperature region, and the curve width is significantly increased. With 0.1wt% Sn doping, the Curie temperature remains constant and ΔS_M slightly increases to 7.38 J/(kg·K). With 0.2wt% Sn doping, the Curie temperature increases to 204 K, the full width at half maximum (δT_{FWHM}) of curve significantly increases, but ΔS_M decreases to 3.69 J/(kg·K).

In addition, RCP of the $La_{0.75}Ce_{0.25}Fe_{11.5-x}Al_{0.2}Si_{1.3}Sn_x$ alloys is calculated by Eq.(2)[41], as follows:

$$RCP = -\Delta S_M \delta T_{FWHM} \quad (2)$$

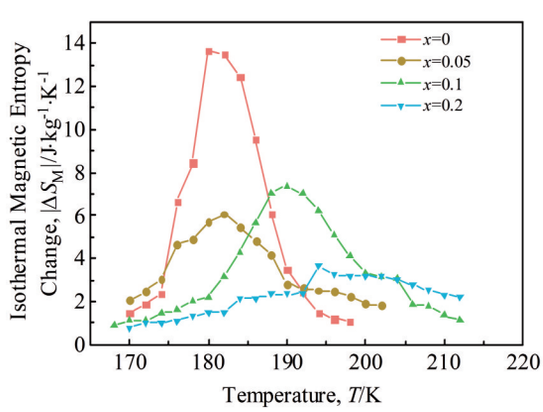

Fig.6 Relationship between isothermal magnetic entropy change and temperature of $La_{0.75}Ce_{0.25}Fe_{11.5-x}Al_{0.2}Si_{1.3}Sn_x$ alloys under magnetic field of 2 T

where RCP represents the heat transfer by the magnetic refrigerant between the hot and cold ends during the magnetic refrigeration cycle; ΔS_M is the peak value of isothermal magnetic entropy change; δT_{FWHM} is calculated by integrating the *M-T* curve under a certain magnetic field. The relative cooling capacities of $La_{0.75}Ce_{0.25}Fe_{11.5-x}Al_{0.2}Si_{1.3}Sn_x$ alloys with x=0, 0.05, 0.1, and 0.2 are 154, 96, 119, and 123 J/kg, respectively. The MCE properties of $La_{0.75}Ce_{0.25}Fe_{11.5-x}Al_{0.2}Si_{1.3}Sn_x$ alloys are shown in Table 2, and they are compared with the results from different reports. RCP value of the $La_{0.75}Ce_{0.25}Fe_{11.3}Al_{0.2}Si_{1.3}Sn_{0.2}$ alloy with low MCE and large δT_{FWHM} reaches 80% of that of the $La_{0.75}Ce_{0.25}Fe_{11.5}Al_{0.2}Si_{1.3}$ alloy with high MCE and small δT_{FWHM}. In addition, the Curie temperature of the $La_{0.75}Ce_{0.25}Fe_{11.5}Al_{0.2}Si_{1.3}Sn_{0.2}$ alloy increases by 15%, the δT_{FWHM} increases by nearly three times, and the thermal hysteresis decreases.

The isothermal magnetization curves of $La_{0.75}Ce_{0.25}Fe_{11.5-x}Al_{0.2}Si_{1.3}Sn_x$ (x=0, 0.05, 0.1, 0.2) alloys at different temperatures with temperature interval of 2 K are shown in Fig.7.

The magnetization of $La_{0.75}Ce_{0.25}Fe_{11.5-x}Al_{0.2}Si_{1.3}Sn_x$ alloys below the Curie temperature rapidly reaches saturation with increasing applied magnetic field, showing typical ferromagnetic-state characteristics. With increasing the temperature, the magnetization of $La_{0.75}Ce_{0.25}Fe_{11.5-x}Al_{0.2}Si_{1.3}Sn_x$ alloys slowly is increased, presenting the transition from ferromagnetic state to paramagnetic state. An obvious S-shaped curve can be observed at x=0 (Fig. 7a), indicating that this alloy has a first-order itinerant electron variable magnetic transition. At x=0.05, 0.1, and 0.2, the main part of isothermal magnetization curves is basically a straight line,

Table 2 Comparison of isothermal magnetic entropy change, Curie temperature, thermal hysteresis, δT_{FWHM}, and RCP of different alloys

Alloy	Isothermal magnetic entropy change, ΔS_M/J·kg^{-1}·K^{-1}	Curie temperature, T_C/K	Thermal hysteresis, ΔT_{hyst}/K	Full width at half maximum, δT_{FWHM}/K	Relative cooling power, RCP/J·kg^{-1}	Ref.
$La_{0.75}Ce_{0.25}Fe_{11.5}Al_{0.2}Si_{1.3}$	13.6	177	1	11.32	154	-
$La_{0.75}Ce_{0.25}Fe_{11.45}Al_{0.2}Si_{1.3}Sn_{0.05}$	6.08	184	0	15.74	96	-
$La_{0.75}Ce_{0.25}Fe_{11.4}Al_{0.2}Si_{1.3}Sn_{0.1}$	7.38	190	0	16.18	119	-
$La_{0.75}Ce_{0.25}Fe_{11.3}Al_{0.2}Si_{1.3}Sn_{0.2}$	3.69	204	0	33.29	123	-
$La_{0.95}Gd_{0.05}Fe_{11.5}Si_{1.5}$	15.3	196	-	9.2	140.2	[20]
$La_{0.85}Gd_{0.15}Fe_{11.5}Si_{1.5}$	9.5	198	-	11.6	110.2	[20]
$La_{1.3}Fe_{11.5}Si_{1.4}Ga_{0.1}$	16.36	188	1.41	-	178.4	[42]
$La_{1.3}Fe_{11.3}Si_{1.4}Ga_{0.3}$	5	200	0.71	-	125.3	[42]
$LaFe_{11.4}Si_{1.6}$	14.3	208	-	-	70	[43]

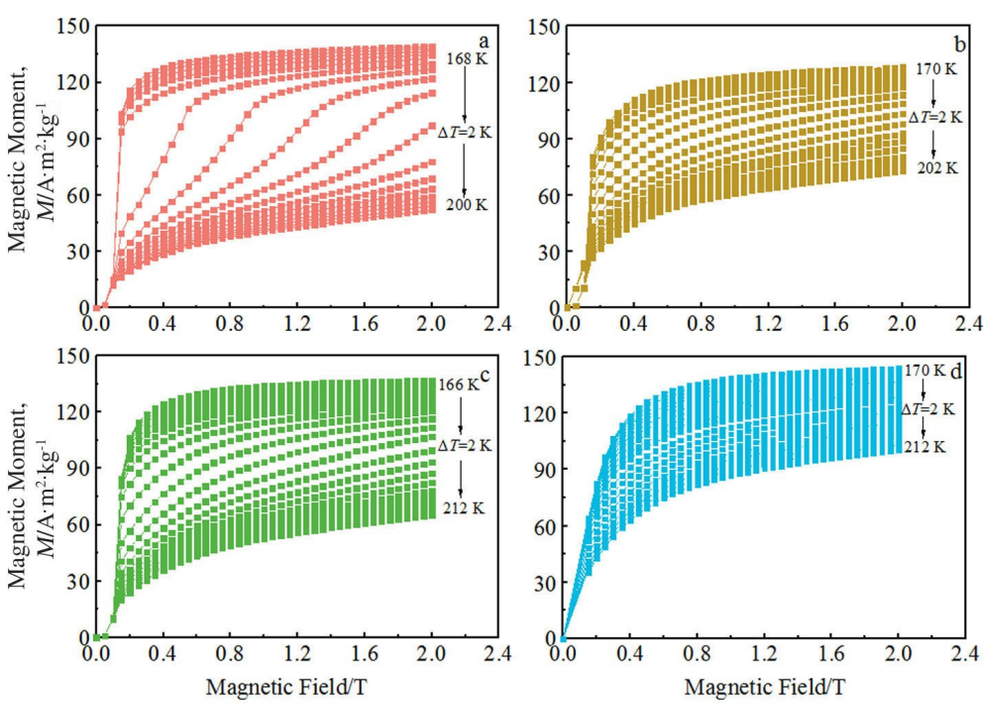

Fig.7 Isothermal magnetization curves of $La_{0.75}Ce_{0.25}Fe_{11.5-x}Al_{0.2}Si_{1.3}Sn_x$ alloys at different temperatures with temperature interval of 2 K: (a) x=0, (b) x=0.05, (c) x=0.1, and (d) x=0.2

and no first-order itinerant electron variable magnetic transition can be observed, as shown in Fig.7b–7d.

The Belov-Arrott plots of $La_{0.75}Ce_{0.25}Fe_{11.5-x}Al_{0.2}Si_{1.3}Sn_x$ (x=0, 0.05, 0.1, 0.2) alloys at the corresponding transition temperatures near Curie temperature are shown in Fig. 8. The magnetic field is represented by $\mu_0 H$.

According to the Banerjee criterion, the magnetic phase transition of $La_{0.75}Ce_{0.25}Fe_{11.5-x}Al_{0.2}Si_{1.3}Sn_x$ alloy can be determined by the slope of M^2-$\mu_0 H/M$ curve[44]. If the curve has an inflection point near the Curie temperature or the slope of the curve is negative, it is suggested that the phase transition is FOPT, and vice versa. The Belov-Arrott plot at x=0 has one inflection point, indicating that this alloy exhibits a strong primary phase transition near the Curie temperature.

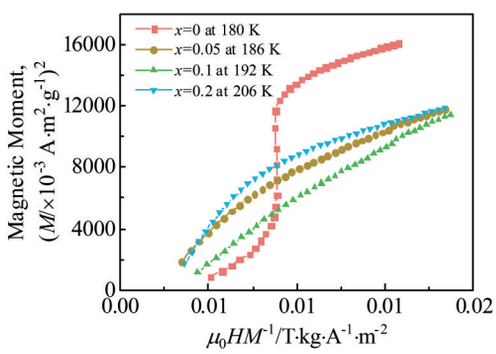

Fig.8 Belov-Arrott plots of $La_{0.75}Ce_{0.25}Fe_{11.5-x}Al_{0.2}Si_{1.3}Sn_x$ (x=0, 0.05, 0.1, 0.2) alloys at corresponding transition temperatures around Curie temperature

Additionally, the Belov-Arrott plots of other alloys show positive slopes, indicating that the variable magnetic-transition behavior of the alloys weakens near the Curie temperature and the secondary phase transition occurs. Therefore, it is concluded that Sn element can induce the secondary phase transitions in the $(La, Ce)(Fe, Al, Si)_{13}$ alloys with significantly low doping contents, compared with Co (0.4wt%) [18], Ni (0.21wt%) [23], Cr (0.53wt%) [24], and Ga (0.3wt%)[42].

Because the Banerjee criterion is based on the assumptions of mean-field model, there are certain restrictions. Therefore, the Law method was proposed to confirm the phase transformation through the field dependence of MCE, and the phase-transformation order of the Sn-doped alloys can be obtained[45]. This approach does not rely on the fitting data of any particular magnetization model or any specific equation of state, and it allows a more objective judgment of phase changes, which has been applied to $La(Fe, Si)_{13}$ [23], Heusler alloys[46], and Ni-Mn-Ga/Al[47] alloys[48].

The relationship between the isothermal magnetic entropy change and the magnetic field obeys the power law of the field, as follows:

$$\Delta S_M \propto H^n \tag{3}$$

where the exponent n represents the function depending on the temperature and field.

$$n = \frac{\mathrm{d}\ln|\Delta S_M|}{\mathrm{d}\ln|H|} \tag{4}$$

When n>2, the phase transition is FOPT. Otherwise, the phase transition is SOPT. The relationship between $\mu_0 H$ and T

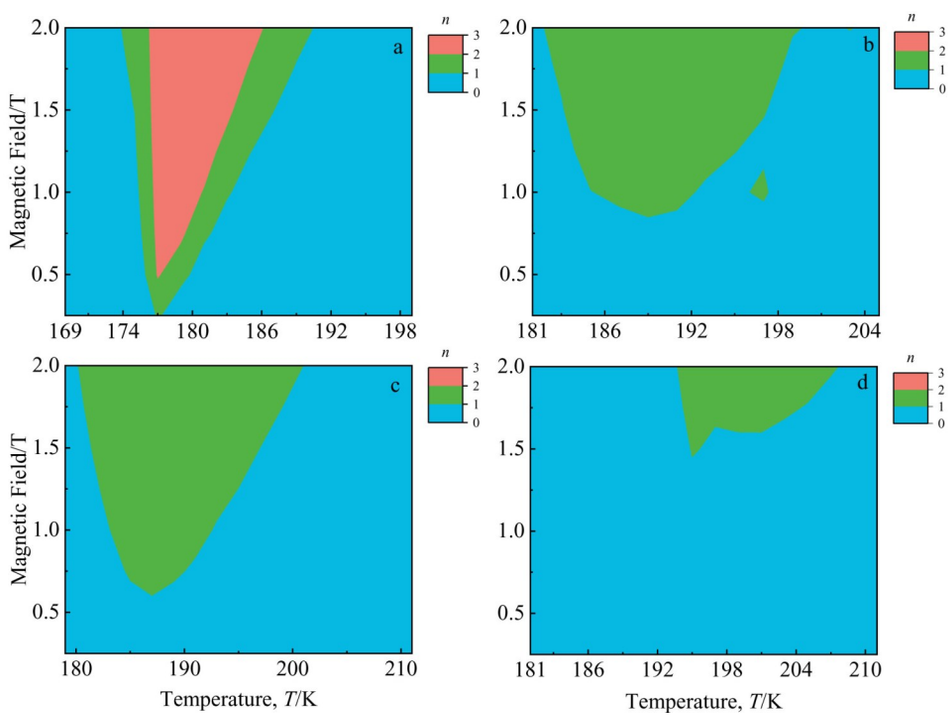

Fig.9 Variation of exponent n of $La_{0.75}Ce_{0.25}Fe_{11.5-x}Al_{0.2}Si_{1.3}Sn_x$ alloys under different magnetic fields and temperatures: (a) x=0, (b) x=0.05, (c) x=0.1, and (d) x=0.2

is shown in Fig. 9, where red represents the region with $n>2$, green represents the region with $n=[1, 2]$, and blue represents the region with $n=[0, 1)$. At $x=0$, there is a red region, indicating that the n value of $La_{0.75}Ce_{0.25}Fe_{11.5}Al_{0.2}Si_{1.3}$ alloy is above 2 and the alloy undergoes FOPT.

With increasing the Sn content from 0.05wt% to 0.2wt%, no red areas (overshoot zones) can be observed (Fig. 9b–9d), indicating that only SOPT occurs in these alloys. According to the Banerjee criterion and the criterion of phase-transition sequence, when the Sn doping content is 0.05wt%, the alloy changes from FOPT to SOPT. Therefore, the doping content of Sn element has a significant effect on the phase transition properties of (La, Ce) (Fe, Al, Si)$_{13}$ alloys. By adjusting the doping content of Sn element, the phase transformation and magnetocaloric properties of the alloy can be adjusted to achieve multi-stage series refrigeration.

3 Conclusions

1) According to the density functional theory calculations, with increasing the Sn doping content, the lattice constant and exchange integral between the Fe-Fe bonds are increased, resulting in the increase in Curie temperature. The simulation results are in good agreement with the experimental ones. Through the traditional Banerjee criterion and the exponent n, it is concluded that the second-order phase transition (SOPT) occurs when the Sn doping content is 0.05wt%. The phase transition behavior of the $La_{0.75}Ce_{0.25}Fe_{11.5-x}Al_{0.2}Si_{1.3}Sn_x$ alloys is very sensitive to the composition change caused by Sn addition, and the required Sn doping content for SOPT occurrence is significantly lower than the doping content of other elements.

2) Sn addition can increase the Curie temperature, widen the magnetic refrigeration temperature range, and reduce the thermal hysteresis. By adjusting the doping content of Sn element, the phase transformation and magnetocaloric properties of the alloy can be adjusted to achieve multi-stage series refrigeration.

3) For the $La_{0.75}Ce_{0.25}Fe_{11.5}Al_{0.2}Si_{1.3}$ alloy, the Curie temperature is 177 K, the magnetic entropy change is 13.6 J/(kg·K), the thermal hysteresis is 1 K, and the relative cooling capacity is 154 J/kg under magnetic field of 2 T. Thus, the $La_{0.75}Ce_{0.25}Fe_{11.5}Al_{0.2}Si_{1.3}$ alloy shows great potential as magnetic refrigeration materials at specific temperatures.

References

1 Kitanovski A. *Advanced Energy Materials*[J], 2020, 10: 1 903 741

2 Fries M, Pfeuffer L, Bruder E *et al*. *Acta Materialia*[J], 2017, 132: 222

3 Porcari G, Morrison K, Cugini F *et al*. *International Journal of Refrigeration*[J], 2015, 59: 29

4 Ram N R, Prakash M, Naresh U *et al*. *Journal of Superconductivity and Novel Magnetism*[J], 2018, 31(7): 1971

5 Franco V, Blázquez J S, Ipus J J *et al*. *Progress in Materials Science*[J], 2018, 93: 112

6 Jaeger G. *Archive for History of Exact Sciences*[J], 1998, 53: 51

7 Nobrega E P, De Oliveira N A, Von Ranke P J *et al*. *Journal of Magnetism and Magnetic Materials*[J], 2008, 320(14): 147

8 Fujieda S, Fujita A, Fukamichi K. *Applied Physics Letters*[J], 2002, 81: 1276

9 Pecharsky V K, Gschneidner K A. *Physical Review Letters*[J], 1997, 78(23): 4494

10 Wada H, Tanabe Y. *Applied Physics Letters*[J], 2001, 79(20): 3302

11 Planes A, Mañosa L, Acet M. *Journal of Physics: Condensed Matter*[J], 2009, 21(23): 233 201

12 Staunton J B, Banerjee R, Dos Santos-Dias M *et al*. *Physical Review B*[J], 2014, 89(5): 54 427

13 Lyubina J, Schäfer R, Martin N *et al*. *Advanced Materials*[J], 2010, 22(33): 3735

14 Dong Q Y, Zhang H W, Chen J *et al*. *Journal of Magnetism and Magnetic Materials*[J], 2013, 331: 183

15 Fujita A, Akamatsu Y, Fukamichi K. *Journal of Applied Physics*[J], 1999, 85(8): 4756

16 Lin Z P, Li S D, Liu M M *et al*. *Journal of Alloys and Compounds*[J], 2010, 489(1): 1

17 Wang G F, Song L, Li F A *et al*. *Journal of Magnetism and Magnetic Materials*[J], 2009, 321(21): 3548

18 Shen B G, Sun J R, Hu F X *et al*. *Advanced Materials*[J], 2009, 21(45): 4545

19 Lu C X, Wu Q M, Wang H F *et al*. *Journal of Alloys and Compounds*[J], 2021, 872: 159 553

20 Yan Y J, Liu C S, Lu W C *et al*. *Journal of Alloys and Compounds*[J], 2022, 910: 164 858

21 Hu F X, Shen B G, Sun J R *et al*. *Journal of Applied Physics*[J], 2007, 101(9): 09C525

22 Dai Y T, Li Y Q, Xu Z S *et al*. *Journal of Alloys and Compounds*[J], 2018, 765: 538

23 Moreno-Ramírez L M, Romero-Muñiz C, Law J Y *et al. Acta Materialia*[J], 2018, 160: 137

24 Moreno-Ramírez L M, Romero-Muñiz C, Law J Y *et al. Acta Materialia*[J], 2019, 175: 406

25 Chen X, Chen Y G, Tang Y B *et al. Transactions of Nonferrous Metals Society of China*[J], 2014, 24(3): 705

26 Hou Xueling, Kong Junfeng, Li Shitao *et al. Rare Metal Materials and Engineering*[J], 2007, 36(9): 1605 (in Chinese)

27 Wang G F, Ren W, Yang B Y. *Intermetallics*[J], 2021, 136: 107 269

28 Perdew J P, Wang Y. *Physical Review B*[J], 1992, 45(23): 13 244

29 Segall M D, Lindan P J D, Probert M J *et al. Journal of Physics: Condensed Matter*[J], 2002, 14(11): 2717

30 Perdew J P, Zunger A. *Physical Review B*[J], 1981, 23(10): 5048

31 Ceperley D M, Alder B J. *Physical Review Letters*[J], 1980, 45(7): 566

32 Gruner M E, Keune W, Landers J *et al. Physica Status Solidi*

B[J], 2017, 255(2): 1 700 465
33 Phejar M, Paul-Boncour V, Bessais L. *Intermetallics*[J], 2010, 18(12): 2301
34 Helmholdt R B, Palstra T T M, Nieuwenhuys G J *et al. Physical Review B*[J], 1986, 34(1): 169
35 Irisawa K, Fujita A, Fukamichi K *et al. Journal of Alloys and Compounds*[J], 2001, 316(1–2): 70
36 Hai X Y, Mayer C, Colin C V *et al. Journal of Magnetism and Magnetic Materials*[J], 2016, 400: 344
37 Liu X B, Altounian Z, Ryan D H. *Journal of Physics: Condensed Matter*[J], 2003, 15(43): 7385
38 Wang F W, Zhang P, Wang J Y *et al. Journal of Magnetism and Magnetic Materials*[J], 1999, 192(3): 485
39 Wang G J, Hu F X, Wang F *et al. Chinese Physics*[J], 2004, 13(4): 546
40 Gercsi Z. *Europhysics Letters*[J], 2015, 110(4): 47 006
41 Fujita A, Fujieda S, Fukamichi K. *Journal of Magnetism and Magnetic Materials*[J], 2007, 310(2): e1006
42 Archana R, Ramakrishna V V, Suresh V *et al. Journal of Superconductivity and Novel Magnetism*[J], 2022, 35(9): 2505
43 Hu F X, Shen B G, Sun J R *et al. Applied Physics Letters*[J], 2001, 78(23): 3675
44 Banerjee B K. *Physics Letters*[J], 1964, 12(1): 16
45 Law J Y, Franco V, Moreno-Ramírez L M *et al. Nature Communications*[J], 2018, 9(1): 2680
46 Law J Y, Díaz-García Á, Moreno-Ramírez L M *et al. Acta Materialia*[J], 2019, 166: 459
47 Zhang Y C, Franco V, Wang Y F *et al. Journal of Alloys and Compounds*[J], 2022, 918: 165 664
48 Romero-Muñiz C, Franco V, Conde A. *Physical Chemistry Chemical Physics*[J], 2017, 19(5): 3582

掺杂Sn对$(La, Ce)(Fe, Al, Si)_{13}$合金磁热效应和相变性质的影响

宋博宇[1,2,3]，韩永全[1,3]，程　娟[4]，高　磊[4]，刘翠兰[4]，黄焦宏[4]
(1. 内蒙古工业大学，内蒙古 呼和浩特 010051)
(2. 包头职业技术学院，内蒙古 包头 014030)
(3. 先进轻金属材料开发与加工防护教育部工程研究中心，内蒙古 呼和浩特 010051)
(4. 白云鄂博稀土资源研究与综合利用国家重点实验室，内蒙古 包头 014030)

摘　要：研究了磁制冷材料$La_{0.75}Ce_{0.25}Fe_{11.5-x}Al_{0.2}Si_{1.3}Sn_x$（$x$=0，0.05，0.1，0.2）的磁热效应和相变性质。X射线衍射结果表明，随着Sn掺杂浓度的增加，主相1:13相减少，α-Fe和LaFeSi相增加。引入密度泛函理论，结合实验结果得出，增加Sn掺杂浓度能够增大晶格常数，并增强相邻原子之间的交换相互作用，从而提高居里温度。当磁场变化为2 T时，体系中最大磁熵变为13.59 $J·kg^{-1}·K^{-1}$，其相对制冷能力为154 J/kg，具有成为磁制冷材料的潜力。通过Banerjee准则和等温熵变的场相关指数n确定当Sn掺杂浓度为0.05%（质量分数）时，合金由一级相变转变为二级相变。合金的相变行为对Sn含量非常敏感，可以通过调节Sn掺杂浓度，实现多级串联制冷。

关键词：磁热效应；LaFeSi；相变

作者简介：宋博宇，女，1983年生，博士，副教授，内蒙古工业大学材料科学与工程学院，内蒙古 呼和浩特 010051，E-mail：Songboyu10-8@outlook.com